Local response of a glacier to annual filling and drainage of an ice-marginal lake

Joseph S. WALDER,[1] Dennis C. TRABANT,[2] Michelle CUNICO,[3] Andrew G. FOUNTAIN,[3] Suzanne P. ANDERSON,[4,5,*] Robert S. ANDERSON,[4,6,*] Andrew MALM[7]

[1]*US Geological Survey, Cascades Volcano Observatory, 1300 SE Cardinal Court, Vancouver, Washington 8683-9589, USA*
E-mail: jswalder@usgs.gov
[2]*US Geological Survey, 3400 Shell Street, Fairbanks, Alaska 99701-7245, USA*
[3]*Department of Geology, Portland State University, PO Box 751, Portland, Oregon 97207-0751, USA*
[4]*Institute of Arctic and Alpine Research, University of Colorado, Boulder, Colorado 80309-0450, USA*
[5]*Department of Geography, University of Colorado, Boulder, Colorado 80309-0260, USA*
[6]*Department of Geological Sciences, University of Colorado, Boulder, Colorado 80309-0399, USA*
[7]*Department of Physics, St Olaf College, 1520 St Olaf Avenue, Northfield, Minnesota 55057-1098, USA*

ABSTRACT. Ice-marginal Hidden Creek Lake, Alaska, USA, outbursts annually over the course of 2–3 days. As the lake fills, survey targets on the surface of the 'ice dam' (the glacier adjacent to the lake) move obliquely to the ice margin and rise substantially. As the lake drains, ice motion speeds up, becomes nearly perpendicular to the face of the ice dam, and the ice surface drops. Vertical movement of the ice dam probably reflects growth and decay of a wedge of water beneath the ice dam, in line with established ideas about jökulhlaup mechanics. However, the distribution of vertical ice movement, with a narrow (50–100 m wide) zone where the uplift rate decreases by 90%, cannot be explained by invoking flexure of the ice dam in a fashion analogous to tidal flexure of a floating glacier tongue or ice shelf. Rather, the zone of large uplift-rate gradient is a fault zone: ice-dam deformation is dominated by movement along high-angle faults that cut the ice dam through its entire thickness, with the sense of fault slip reversing as the lake drains. Survey targets spanning the zone of steep uplift gradient move relative to one another in a nearly reversible fashion as the lake fills and drains. The horizontal strain rate also undergoes a reversal across this zone, being compressional as the lake fills, but extensional as the lake drains. Frictional resistance to fault-block motion probably accounts for the fact that lake level falls measurably before the onset of accelerated horizontal motion and vertical downdrop. As the overall fault pattern is the same from year to year, even though ice is lost by calving, the faults must be regularly regenerated, probably by linkage of surface and bottom crevasses as ice is advected toward the lake basin.

INTRODUCTION

A jökulhlaup, or glacial outburst flood, is caused by sudden release of water impounded by a glacier either subglacially or subaerially, in the latter case commonly at the confluence of two glaciers or in a deglaciated tributary valley (Post and Mayo, 1971). Previous studies of jökulhlaups have typically focused on measurements of, or inferences about, the flood hydrograph, with many data being either serendipitous or based on approximate, after-the-fact methods common to flood hydrology (see review by Walder and Costa, 1996). Such hydrologically focused studies have served as the background against which investigators have developed physically based models of jökulhlaups and schemes (largely empirical) for predicting flood–hydrograph characteristics (e.g. Clague and Mathews, 1973; Björnsson, 1974, 1992; Nye, 1976; Walder and Costa, 1996; Fowler, 1999; Ng and Björnsson, 2003; Roberts, 2005). A related body of literature deals with fluvial sediment transport during jökulhlaups (e.g. Old and others, 2005) and the geomorphic effects of these events (e.g. Russell and others, 2002). The present study instead examines one key aspect of glacier behavior during the jökulhlaup cycle at an ice-dammed lake – an aspect that has hitherto generally been regarded as a passive actor in the jökulhlaup 'system', namely deformation of the ice dam. (We use 'ice dam' to refer to the part of the glacier adjacent to the lake.)

Although our focus is not the mechanism of jökulhlaup triggering (which presumably requires breaching of a drainage divide at the bed beneath the ice dam), consideration of this mechanism was highly relevant in motivating our study. Discussions of jökulhlaup initiation commonly (albeit not always; see Roberts, 2005) involve the hypothesis that an ice dam progressively becomes afloat as a wedge of lake water penetrates beneath the glacier (Fig. 1), a scenario dubbed an 'inverted cantilever' by Nye (1976, p. 186–7), who argued that because isostatic adjustment is not instantaneous, the ice dam would 'be subject to a buoyancy force which will bend it upwards.' With Nye's picture of the physical situation in mind, we began this study expecting to find that a growing, then shrinking, subglacial water wedge would cause the ice dam to deform by flexure, as does an ice shelf or a floating tidewater glacier in response to ocean tides (e.g. Lingle and others, 1981). The data turn out to be inconsistent with our expectation: the ice dam indeed deforms as the lake fills and drains, but this deformation is dominated by high-angle reverse and normal faulting. This

*Formerly at: Department of Earth Sciences, University of California, Santa Cruz, 1156 High Street, Santa Cruz, Californaia 95064, USA.

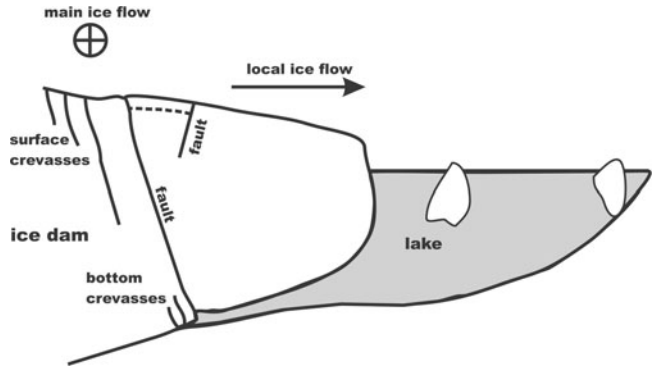

Fig. 1. Schematic cross-section illustrating an ice dam progressively becoming afloat as a wedge of water lifts the ice off the bed. As envisaged by Nye (1976), nearly floating ice acts as an 'inverted cantilever' to pry ice from the bed at the thin edge of the subglacial water wedge. In an alternative conceptual framework that is developed in this paper, mechanical behavior of the ice dam is instead dominated by faults, some of which cut the ice dam from surface to bed. The dotted line represents downdrop of part of the glacier surface owing to graben development as the ice dam stretches during lake drainage.

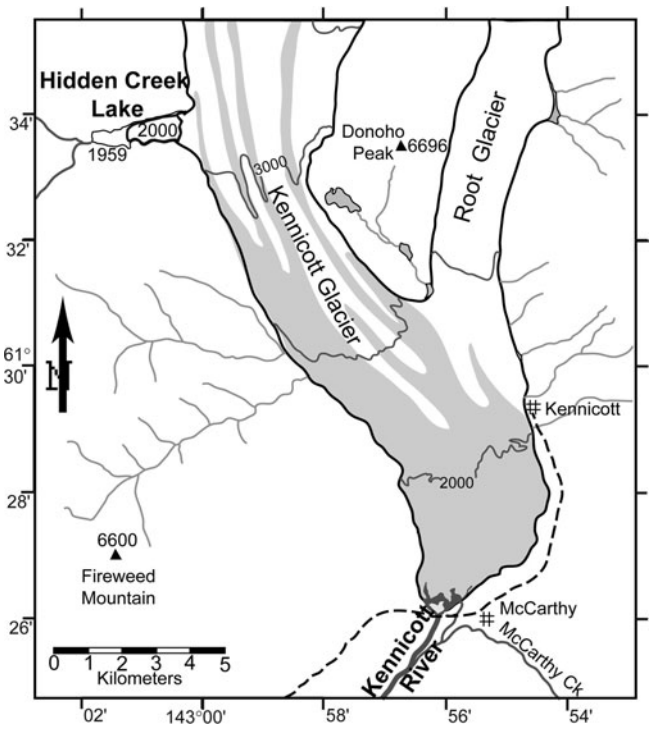

Fig. 2. Index map of field area, simplified from US Geological Survey topographic map. Elevations are in feet (1 ft = 0.305 m), and the contour interval on the ice surface is 500 ft (152 m). Stippled pattern indicates debris cover. Maximum extent of Hidden Creek Lake in 1959 and 2000 is indicated.

mode of deformation is not commonly associated with glaciers except for collapse features in ice overlying sites of subglacial basaltic eruptions (e.g. Björnsson, 2002, p. 261).

The present paper expands upon a condensed discussion of ice-dam mechanics given by Walder and others (2005). The connection between lake drainage and glacier sliding has been explored by Anderson and others (2005); hydrologic and hydrochemical observations of the associated jökulhlaups have been reported by Anderson and others (2003a, b). A recent project at Gornersee, Switzerland, to date reported only in abstracts (Sugiyama and others, 2005; Huss and others, 2006; Werder and others, 2006), promises to yield important further data on the mechanical coupling between ice-dammed lakes and the glaciers that impound them.

FIELD SITE

We investigated the ice dam that impounds Hidden Creek Lake (HCL), which forms annually in the valley of Hidden Creek at a distance of about 16 km from the terminus of Kennicott Glacier, Wrangell Mountains, south-central Alaska, USA (Fig. 2). The Hidden Creek valley is a deglaciated tributary to Kennicott Glacier. The HCL 'ice dam' is, for our purposes, taken as the part of the glacier that intrudes (by about 800 m) up the valley of Hidden Creek. HCL drains every summer after attaining a surface area of about 1 km^2, a depth near the ice dam of about 100 m and a volume of about $20–30 \times 10^6$ m^3. Our ability to anticipate the approximate date of lake drainage was central to our being able to collect an appropriate suite of hydrologic and geodetic data. During the roughly 90 years for which a record exists, the date of drainage has shown a definite trend from late to early summer, with a correspondingly smaller lake area and volume at the time of drainage. This temporal trend correlates with reduction in extent and (presumably) thickness of the glacier. Additional background information about HCL and Kennicott Glacier may be found in Friend (1988), Rickman and Rosenkrans (1997) and Anderson and others (2003a, b).

The surface of the HCL ice dam is partly covered by bands of morainal material and spanned by open fractures, commonly concave towards the lake (Fig. 3); travel on the surface of the ice dam is quite difficult, and the debris content of the ice made hot-water borehole drilling extremely difficult (Anderson and others, 2003a). Ice thickness near HCL, determined from radar measurements described later, reaches about 350 m.

FIELD METHODS

The history of observed HCL jökulhlaups (Rickman and Rosenkrans, 1997) was used as a reference for scheduling fieldwork. In 1999, HCL reached maximum level only a few hours after we reached the field site on day 195 (14 July). We placed nine survey targets on the ice dam and made measurements until the middle of day 201 (20 July). In 2000, when the jökulhlaup began 3 weeks after we started data collection, we surveyed an array of 22 targets four to six times per day from day 186 (4 July) until day 210 (28 July). Distribution of targets on the ice dam (Fig. 4) was uneven owing to challenging ice-surface conditions. The survey base station was set up in both years on a bedrock knob north of the ice dam. Absolute position of the base station in Universal Transverse Mercator (UTM) coordinates was determined using a global positioning system (GPS), with the GPS base station positioned on a US Geological Survey benchmark located about 18 km away, near the village of McCarthy, Alaska. The error in target displacement is about 15 mm, compared to total displacement of at least several meters in both the horizontal and the vertical for most targets (Cunico, 2003).

Fig. 3. Photograph taken from survey instrument site, looking south, in July 2000. HCL is out of view to the right. Some survey-target locations are indicated. Dashed curve is approximate boundary of ice lost by calving (primarily in a single event on day 199). Note water in fractures at lower right.

Lake level in HCL was monitored using pressure transducers placed in the lake using a small inflatable boat, supplemented in 2000 by optical surveying when transducers were destroyed by calving ice. Lake level was referenced to the same GPS datum as were survey measurements. The methods are described more fully in Anderson and others (2003a).

Ice thickness was measured using an ice-penetrating radar system operated at either 5 or 10 MHz. Transmitting and receiving antennae were separated at their centers by a distance of 60 m, with 256 measurements stacked at each point to improve the signal-to-noise ratio. Glacier-surface conditions restricted the radar operator to making spot measurements along rows of seracs and morainal stripes (Fig. 4). Radar soundings were made about every 10 m, with the position of the measurement determined by surveying about every 50 m; the position of intermediate soundings was determined by linear interpolation between surveyed positions. The error in inferred ice thickness is about 5 m near the middle of the ice dam and about 10 m near the margins.

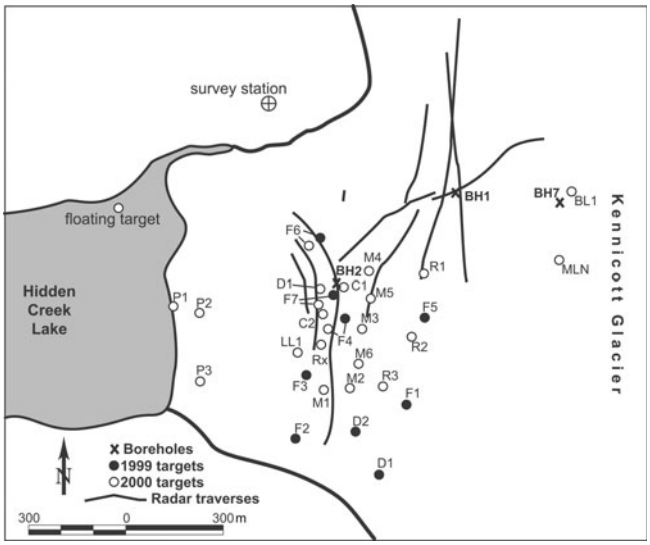

Fig. 4. Map of field area showing radar-measurement transects (solid curves) and locations of survey targets and boreholes. Borehole records were discussed by Anderson and others (2003a).

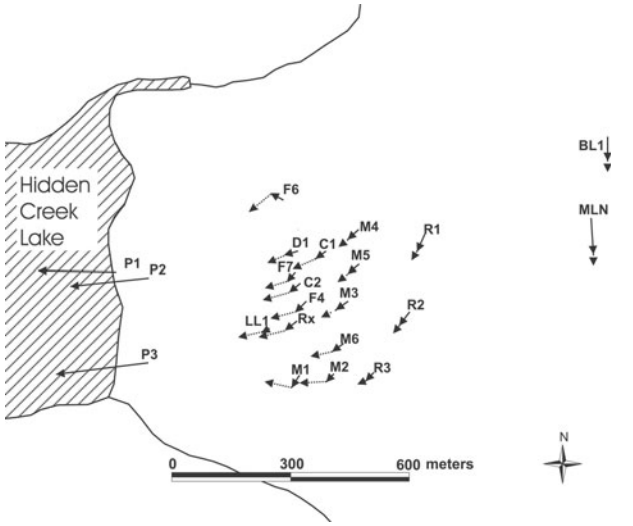

Fig. 5. Average motion vectors for survey targets in 2000. Length is approximately proportional to speed. Solid line gives average trend from start of measurement until azimuth shifted at time τ_1 during lake drainage (see Table 1); dashed line gives average trend thereafter.

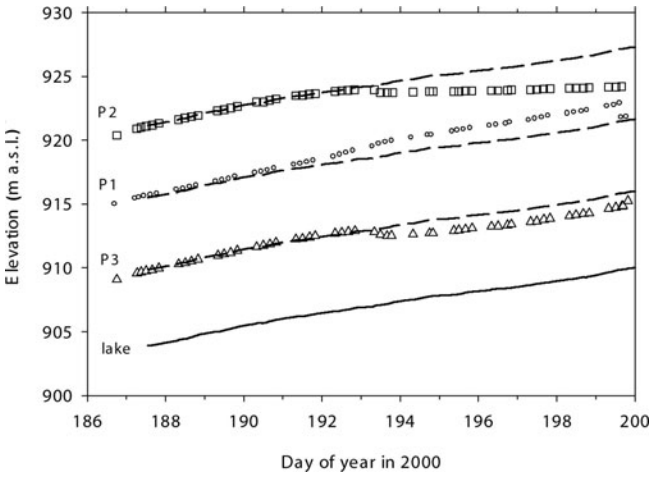

Fig. 6. Vertical-movement history of near-lake targets. Error is about 20 mm. Dashed curves represent lake-level record shifted along the ordinate for ease of comparison with target-movement histories.

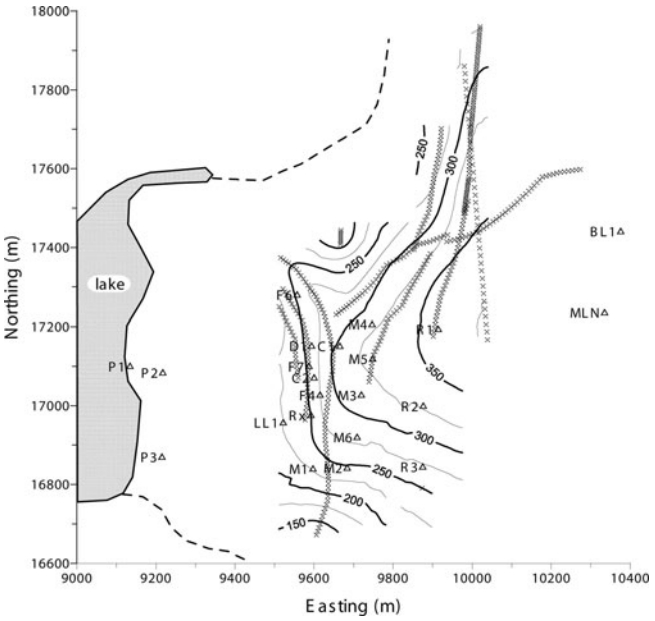

Fig. 7. Ice thickness as derived from radar measurements. Contours are ice thickness in meters. Positions of 2000 survey targets (△) and radar measurements (×) are indicated. Glacier margins are indicated by the dashed curves.

RESULTS

Target movements in 2000

As ice moves southward past the bedrock knob on which our survey station was placed, a portion of the flow diverts westward into the HCL basin (a hanging valley), as is nicely shown by the overall pattern of target trajectories (Fig. 5). The 22 survey targets are separated, for convenience, into three sets based on their general placement. The 'main-glacier' targets BL1 and MLN, located about 1.2 km east of HCL, were relatively little affected by the presence of the lake: they moved nearly due south throughout the observation period, with a speed-up and slight change in azimuth as the lake drained. The main-glacier targets also underwent a vertical displacement that Anderson and others (2005) interpreted in terms of basal water storage and separation of the glacier from its bed. The three 'near-lake' targets P1–P3, all placed by helicopter within 100 m of the edge of the ice dam and eventually lost by calving, must have been on floating ice when our surveying began, as target elevation, $h(t)$, faithfully tracked lake level, $z_l(t)$, until some time on day 192 (Fig. 6). Interestingly, as $h(t)$ began to deviate from $z_l(t)$, the near-lake targets displayed diverse behavior: P2 and P3 deviated downward while P1 deviated upward. The likeliest explanation for this pattern is that targets were on a rotating ice block. More generally, we infer that the near-lake ice was only weakly coupled to the rest of the ice dam. In what follows, we focus on the remaining 17 targets, which we call the 'central cluster' (CC), which sat on ice ~250–350 m thick (Fig. 7).

The displacement of all CC targets had a significant lakeward component throughout the study period, although the magnitude of that component changed over time. The azimuth, ϕ, of every target's displacement was nearly constant until 1 or 2 days after HCL reached peak stage. Target trajectories shifted and targets sped up as the lake drained (Figs 5, 8 and 9). In most cases azimuth, and in all cases horizontal speed, u, changed markedly as the lake drained, with ϕ generally rotating toward the embayment that had formed by calving on day 199 (Fig. 3). (Interestingly, the calving event of day 199 *itself* did not affect either ϕ or u.) The time, τ_1, at which the change in ϕ and/or u occurred was generally earlier on the west side of the CC than on the east side (Table 1). The magnitude of the speed-up decreased with distance from the lake (Fig. 9). Target speed prior to lake drainage displayed diurnal variation (Fig. 9), a phenomenon commonly attributed to basal sliding modulated by the state of the basal drainage system (e.g. Van der Veen, 1999, p. 96–102). However, it seems likely that in

Table 1. Target motion summary in 2000 (maximum lake level at day 206.7)

Target	Initial local easting	τ_1	τ_2	Δh_{drop}
	m	day of year	day of year	m
LL1	9522.36	207.83	207.50	21.11
F6	9556.79	207.8	207.34	11.16
F7	9586.83	207.84	207.25	14.09
Rx	9591.96	207.83	207.50	15.24
D1	9593.91	207.84	207.59	12.21
M1	9597.04	207.83	207.50	14.35
C2	9600.32	207.84	207.50	13.19
F4	9614.59	207.84	207.34	12.84
C1	9664.64	207.84	207.60	2.35
M2	9683.61	207.84	207.71	3.31
M6	9709.12	208.84?	208.84	2.17
M3	9720.47	209.34?	208.84	1.68
M4	9747.06	208.68?	208.77	0.95
M5	9748.02	208.84?	208.84	1.20
R3	9785.05	209.34	209.26	1.31
R2	9875.78	208.35, 209.43	208.81	1.15
R1	9913.95	209.4?	208.81	0.64

Notes: Easting and northing are given relative to an origin at UTM zone 10 coordinates (380000, 6810000). The North American Datum of 1983 was used as the horizontal datum, and the National Geodetic Vertical Datum of 1929 was used for the vertical datum. Error in position is about 0.01 m.
τ_1: approx. time at which speed and/or azimuth of motion changed.
τ_2: approx. time at which apparent storage reached maximum value.
Δh_{drop}: decline in target elevation from maximum to last data point.

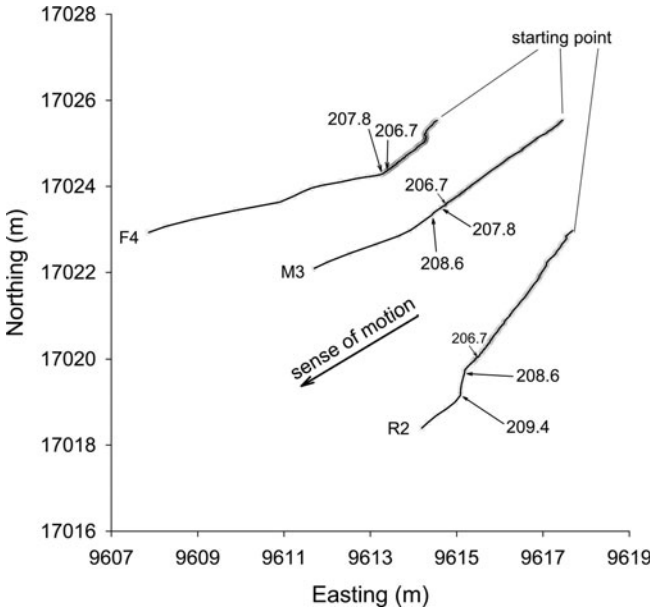

Fig. 8. Trajectories of three CC targets that were roughly oriented in a line normal to the ice-dam face. To show all three trajectories in an undistorted figure, the initial position of M3 has been shifted west by 103 m, while the initial position of R2 has been shifted north by 25 m and west by 258 m (cf. Fig. 5). Positions have been interpolated to 0.2 day intervals. Local easting and northing are relative to UTM zone 10 coordinates (380000, 6810000). Times of peak lake stage (206.7) and of changes in trend of motion are indicated. Other examples are given in the supplemental materials (http://vulcan.wr.usgs.gov/Projects/Walder).

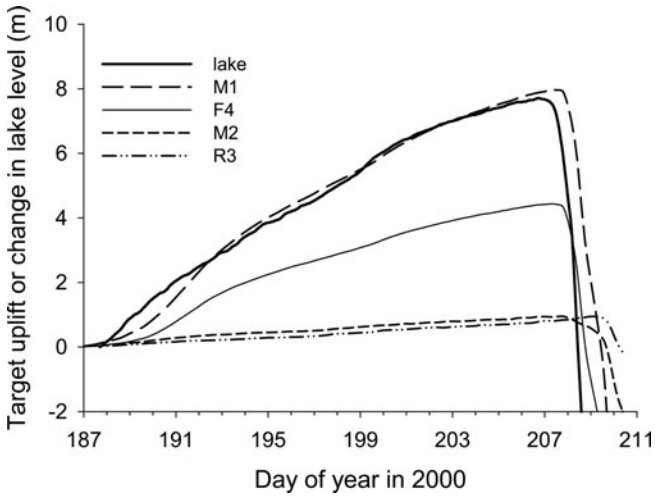

Fig. 10. CC target uplift (corrected for gross glacier flow) and change in lake level as a function of time relative to the start of data collection. Error in target uplift is ~20 mm. Level of HCL is from Anderson and others (2003a) with error ~40 mm.

the present case, what lies at the base of the ice beneath the CC targets is not a 'drainage system' at all, but rather a wedge-like extension of HCL (Anderson and others, 2003a). We return to this point later.

CC targets exhibited diverse vertical motions during lake filling and drainage. As we are interested in vertical motion driven by lake-level change, we must remove from Δh_s, the change in target elevation over time, whatever vertical movement is caused simply by advection of the associated survey targets. We do this by subtracting from Δh_s the quantity Δh_g defined by

$$\Delta h_g = \frac{\partial h}{\partial E}\Delta E + \frac{\partial h}{\partial N}\Delta N, \quad (1)$$

where $h(E, N)$ is the ice-surface elevation as a function of easting E and northing N and ΔE, ΔN are displacements during an increment of time, Δt. We chose for $h(E, N)$ a best-fit planar surface corresponding to the starting target positions ($\partial h/\partial E = 0.061$, $\partial h/\partial N = 0.011$). The corrected elevation change, $\Delta h_s - \Delta h_g$, will be denoted Δh_l. The magnitude of $\Delta h_l(t)$ generally decreased with distance from the lake (Fig. 10). This trend is also illustrated by Figure 11, which shows accumulated vertical rise of CC targets for one particular interval during the period of rising lake level, as well as the total drop, Δh_{drop}, in CC target elevation from the time of peak $\Delta h_l(t)$. The downdrop pattern obviously mimics the uplift pattern, with targets east of F4 dropping

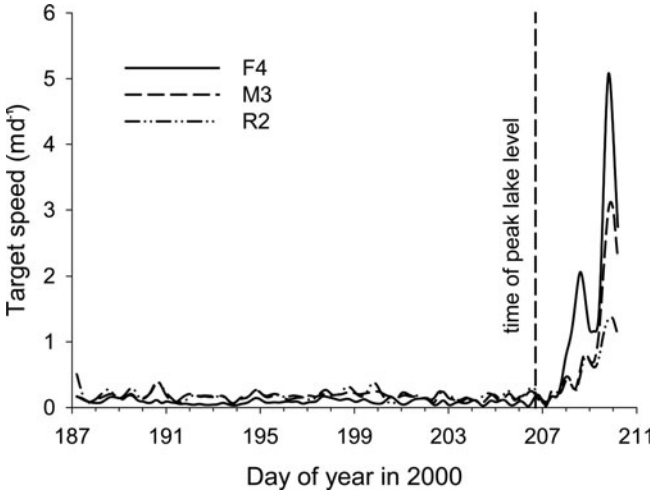

Fig. 9. Speed of the targets whose trajectories are shown in Figure 8. Peak lake stage was reached at day 206.7. Error is ~0.05 m d^{-1}. See supplemental materials for other examples (http://vulcan.wr.usgs.gov/Projects/Walder).

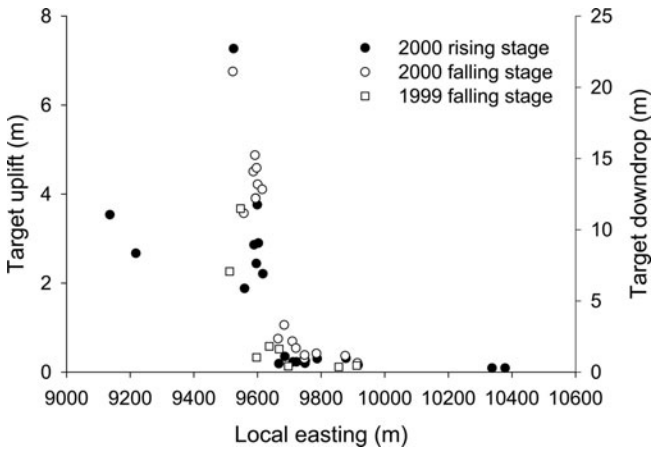

Fig. 11. Target uplift and downdrop as a function of easting. Uplift shown is the accumulated value from the start of data collection in 2000 until the calving event of day 199.7. (Lake level rose 3.6 m during this period.) Downdrop is the difference between maximum value of Δh_s and the last measured value, for both 1999 and 2000.

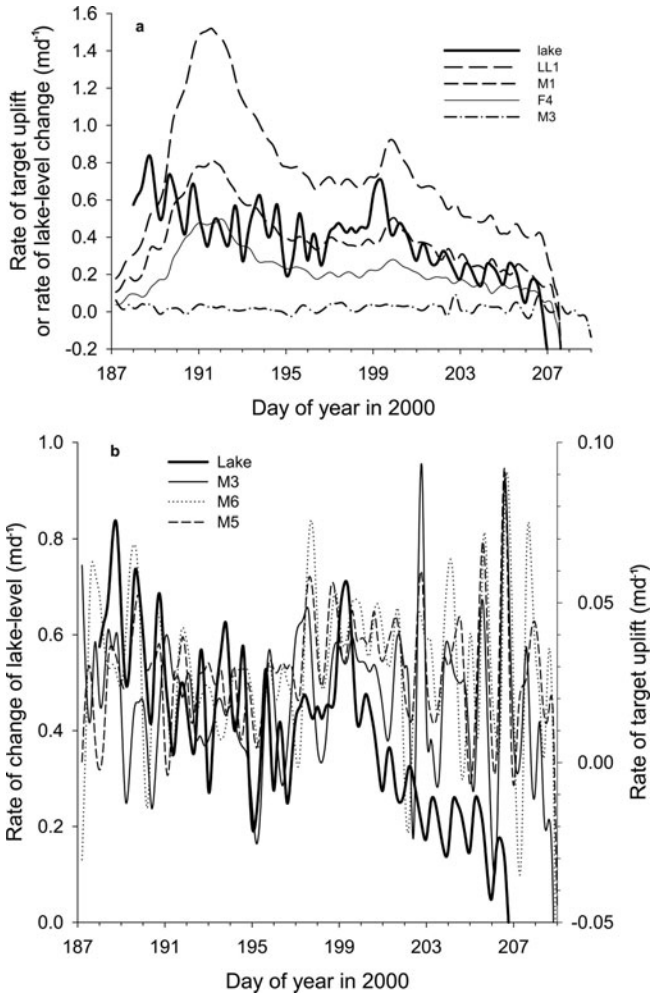

Fig. 12. Uplift rate for representative targets within the CC compared to the rate of change of lake level. (a) Three western subset targets plus, for comparison, M3 from the eastern subset; (b) three eastern subset targets. Uplift rate was determined by applying a three-point running average to vertical position, interpolating to a 0.2 day interval, and then calculating the derivative using a centered difference; the error is about 0.05 m d^{-1}. Note scale difference between panels. See supplemental materials for other examples (http://vulcan.wr.usgs.gov/Projects/Walder).

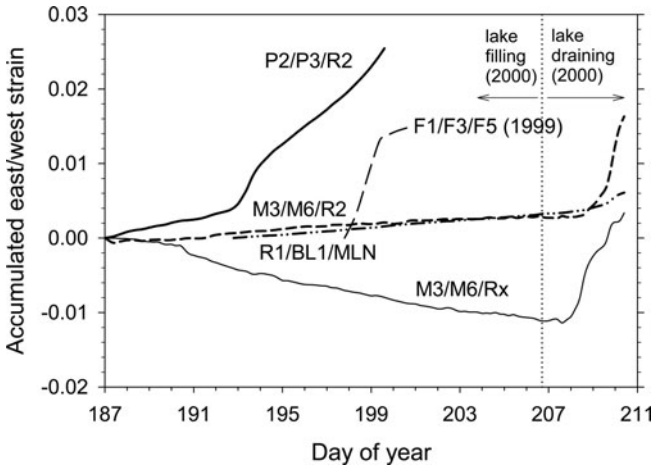

Fig. 13. Accumulated strain in east–west direction relative to the start of data collection, for four triangular elements in 2000 and one in 1999 (see Fig. 4). Error is about 10^{-4}. Extension is positive. For 2000, element P2/P3/R2 is representative of strain rate for the ice dam as a whole up to the time that P2 and P3 were lost by calving; M3/M6/Rx is an element that spans the transition from the western CC to the eastern CC; M3/M6/R2 is an element within the eastern CC; R1/BL1/MLN is a far-field element in a domain that showed very little vertical uplift during lake filling. Element F1/F3/F5 in 1999 is an element analogous to M3/M6/Rx in 2000. See supplemental material for other strain data (http://vulcan.wr.usgs.gov/Projects/Walder).

only about 5–10% as much as F4 and those farther west. Targets did not begin to drop until some time, τ_2, *after* the time of maximum lake level, and close to τ_1, the time at which the change in direction of motion occurred (Table 1).

Comparison of $\partial(\Delta h_l)/\partial t$ (henceforth 'uplift rate') with the rate of lake-level rise, dz_l/dt, reveals the extent to which the ice dam is locally floating. Western (F6, D1, F7, C2, F4, Rx, LL1 and M1) and eastern (C1, M2, M3, M4, M5, M6, R1, R2 and R3) CC-target subsets behave differently in this regard (Fig. 12). Initially, uplift rate was uniformly less than dz_l/dt for targets in the western CC subset, but caught up with, or even exceeded, dz_l/dt beginning on about day 190. Indeed, for target LL1, uplift rate exceeded dz_l/dt nearly continuously from day 190 until the lake drained. A plausible interpretation is that we serendipitously began our measurements just as the section of ice on which LL1 (and perhaps M1) sat was becoming ungrounded. In comparison, uplift rate was always less than dz_l/dt for several targets in the eastern CC subset. The diurnal fluctuation in uplift rate for these targets continued after the lake began to drain (Fig. 12b). The implication is that $\Delta h_l(t)$ depends in some fashion on overall glacier dynamics, and not merely on lake level. We note this explicitly because it is tempting to adopt a conceptual model of a sort of inverted cantilever (cf. Nye, 1976), with $\Delta h_l(t)$ simply driven by water pressure on the bottom of the cantilever (meaning, physically, in the subglacial water wedge). As lake level, $z_l(t)$, is obviously a proxy for water pressure, $\Delta h_l(t)$ should, in this view, depend upon $z_l(t)$ as mediated by the mechanical properties of the ice dam, independently of glacier dynamics. However, the data contradict this view.

When we examine relative target movements, we see that the ice dam was, on average, stretching in an east–west direction (that is, strain rate $\dot{\varepsilon}_{xx} > 0$) at all times (Fig. 13). This is unsurprising: separation between glacier and bed made the ice dam behave similarly to a confined floating ice shelf (Van der Veen, 1999). However, within the narrow transition zone from western-CC to eastern-CC targets, $\dot{\varepsilon}_{xx}$ changed sign over the course of the observation period, being negative as the lake filled, but positive as the lake drained. In other words, western-CC targets reversed their direction of motion relative to eastern-CC targets as the lake drained. Most of these relative-motion trajectories exhibit a very steep plunge toward the lake, at roughly 10° from the vertical (Fig. 14a). Except for one case (relative motions involving LL1; Fig. 14b), which we discuss later, the motion reversal involved targets first approaching one another as the lake rose, then diverging, usually not long after lake level began to drop. The zone of strain and motion reversal coincides with the zone in which the magnitude of the uplift gradient $\partial(\Delta h_s)/\partial x$ was large (Fig. 11). In comparison, relative-motion trajectories for target pairs wholly within the eastern CC do not display motion reversals (Fig. 14c), and east–west strain rate within that zone was at all times extensional (Fig. 13).

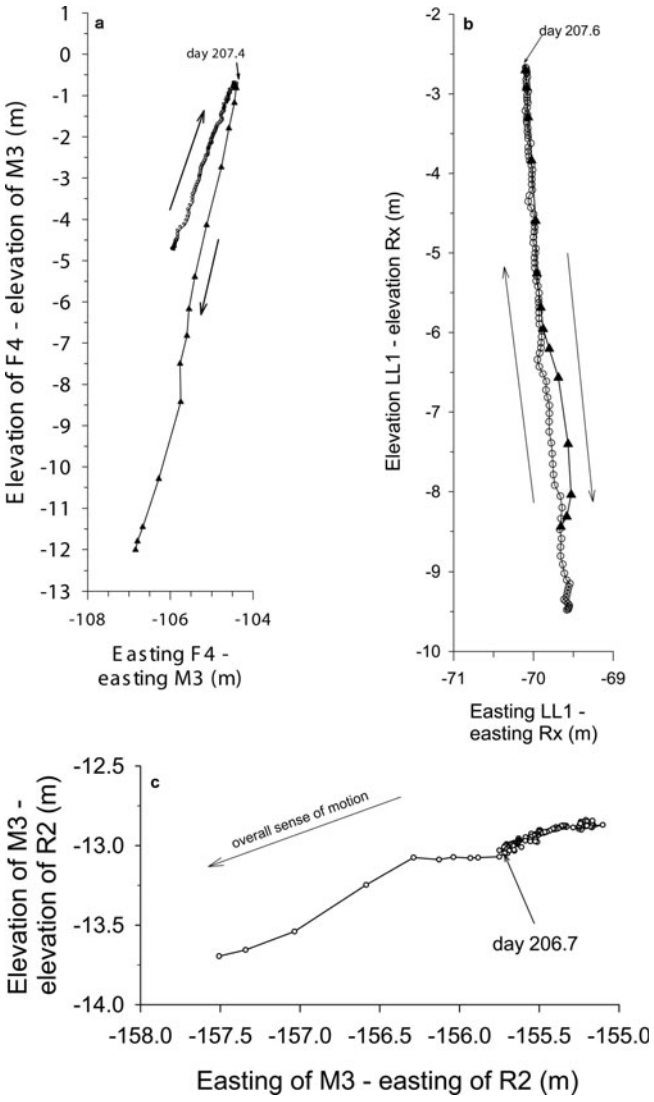

Fig. 14. Relative vertical motions. (a) F4 relative to M3 (spans fault zone); (b) LL1 relative to Rx; and (c) M3 relative to R2. Arrows indicate direction of motion. Error in relative motions is about 40 mm. See supplemental material for other pertinent examples (http://vulcan.wr.usgs.gov/Projects/Walder).

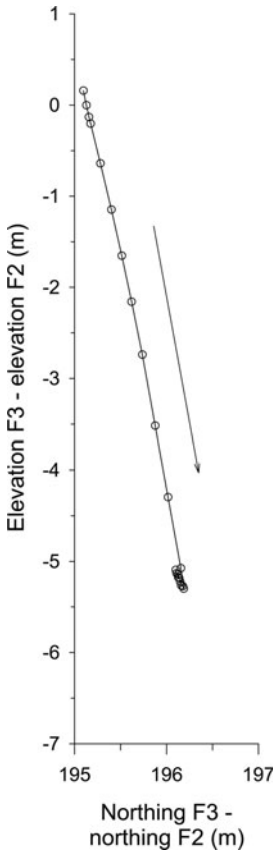

Fig. 15. Relative motion trajectory during drainage in 1999. Arrow indicates direction of motion.

Target movements in 1999

The nine targets deployed in 1999 lay within roughly the same area as the CC targets of 2000 (Fig. 4). The total drop in target elevation, Δh_{drop}, during lake drainage is summarized in Figure 11 and Table 2. The two targets nearest the lake (F2 and F3) dropped significantly more than the rest. The largest measured downdrop in 1999 (at F3) was about 10 m less than in 2000 (at LL1), probably not coincidentally, as the maximum lake level was about 9 m lower in 1999 than in 2000 (Anderson and others, 2003a). Lack of data during rising lake level in 1999 makes identifying the start of downdrop more difficult than with the 2000 data. Nonetheless, it seems clear that, as in 2000, downdrop of the ice surface was delayed relative to the time at which lake level began to drop, with the delay generally increasing with distance from the lake (Table 2) in a way similar to that observed in 2000. Although lack of any data as the lake filled makes it impossible to assess whether the characteristic relative motion reversals seen in 2000 (Figs 13 and 14) also occurred in 1999, trajectories of relative motion between some targets exhibit a very steep plunge (Fig. 15). The limited horizontal-motion data for 1999 are given for completeness in supplemental materials (http://vulcan.wr.usgs.gov/Projects/Walder).

DISCUSSION

Faulting, not flexure

Our data present a detailed picture of the local response of a glacier to filling and drainage of a marginal ice-dammed lake. To the extent that our survey target networks overlapped in 1999 and 2000, motion data for the two years are quite similar: (1) In both years, vertical motions were much greater for targets at an easting of about 9600 than for others only about 100 m farther east. The zone of large $|\partial \Delta h_{\mathrm{l}}/\partial x|$ coincides with a locally large gradient in ice thickness (cf. Figs 7 and 11). (2) Lake drainage and ice-surface lowering were accompanied by rapid extension of the ice in a roughly east–west direction, with the strain rate reaching about 0.01 d^{-1} (Fig. 13). (3) Trajectories of relative motion between targets for some target pairs plunged steeply toward the lake (Figs 14 and 15).

The decrease in ice-surface uplift with increasing distance from the lake is the general pattern one would expect if the ice dam were behaving mechanically as a plate in flexure (e.g. Lingle and others, 1981). However, a flexural explanation of our data faces the fundamental problem that there were two regions of fairly gentle gradient ($\partial \Delta h_{\mathrm{s}}/\partial x$) in vertical displacement separated by a narrow zone, perhaps 50 or 100 m wide, in which the magnitude of $\partial \Delta h_{\mathrm{s}}/\partial x$ was much greater (Fig. 11). This distribution of $\partial \Delta h_{\mathrm{s}}/\partial x$ cannot

Table 2. 1999 target motion summary (maximum lake level at about day 196.0)

Target	Initial local easting	τ_2	Δh_{drop}
	m	day of year	m
F2	9512.26	~197.4	7.07
F3	9546.66	~197.4	11.49
F6	9596.89	197.58/198.6	1.03
F7	9636.93	197.67/198.6	1.81
F4	9667.96	197.87/198.6	1.62
D2	9696.7	198.59	0.41
D1	9766.76	–	–
F1	9855.85	198.59	0.36
F5	9912.32	198.59	0.46

Note: Datum for local easting and northing as in Table 1. Error in position is about 0.01 m.
τ_2: approx. time at which apparent storage reached maximum value.
Δh_{drop}: decline in target elevation from maximum to last data point.

Fig. 16. Kaskawulsh Glacier ice dam in 1986. Photograph by F. Jones, University of British Columbia.

be reproduced by any flexural model unless the flexural rigidity of the ice within a very narrow domain is orders of magnitude less than that of the ice both closer to, and farther from, the lake. A simple scaling argument suffices to make this point. Flexure of the HCL ice dam, like flexure of an ice shelf or floating glacier tongue, say (e.g. Lingle and others, 1981), should be more or less analogous to bending of an elastic plate. Uplift should fall off exponentially with a characteristic length scale, α, given by (cf. Turcotte and Schubert, 1982)

$$\alpha/H_i = [4cY/(\rho_w - \rho_i)gH_i]^{1/4}, \quad (2)$$

where c is a numerical constant typically of order 0.1, Y is Young's modulus for ice and H_i is a characteristic ice thickness, say $H_i = 300$ m (Fig. 7). For the pattern shown in Figure 11 to be explicable by a flexural model, we would require $\alpha \leq 100$ m, so that $\alpha/H_i \leq 1/3$. From Equation (2) we then compute $Y \approx 10$ kPa, whereas actual glacier ice has $Y \approx 10$ GPa (e.g. Lingle and others, 1981). Clearly, a flexural model cannot explain the data.

We believe that our data are most easily understood in terms of movement along high-angle faults that dip towards the lake and cut through the ice dam (Fig. 1). In this interpretation, at least some of the crevasses cutting across the ice dam from north to south (Fig. 3) are simply the surface expression of such faults. We suggest that when the lake fills sufficiently, fault-bounded sections of the ice dam go afloat. Targets separated by such a fault accordingly converge in an east–west direction: motion across the fault is in a reverse (thrust) sense. As the lake drains and the subglacial wedge of water thins beneath the floating sections of the ice dam, those sections sag, and targets separated by a fault diverge in an east–west sense: motion across the fault is in a normal sense. Relative motion trajectories (Figs 14 and 15) are interpreted most simply in terms of (at least) two high-angle, westward-dipping faults: one, exposed at the glacier surface at an easting of about 9650, separated (in year 2000) targets F6, D1, F7, C2, F4, Rx, LL1 and M1 from targets C1 and M2; another, exposed at the glacier surface at an easting of about 9700, separated C1 and M2 from M3, M4, M5 and M6. However, the relative motion of, say, M3 and R2 (Fig. 14c) shows none of the reversibility that we have attributed to faulting, so we conclude that high-angle movement along the fractures evident at the glacier surface is probably negligible east of about easting 9800.

High-angle faulting in ice occurs during subsidence and cauldron formation associated with subglacial volcanism (e.g. Björnsson, 2002, p. 261; Guðmundsson and others, 2004), but the sense of displacement is always normal, never reverse. Mechanical behavior similar to that of the HCL ice dam has been observed at a marginal ice-dammed lake at Kaskawulsh Glacier, Canada, in a setting quite similar to that of HCL at Kennicott Glacier (Kasper, 1989). The part of Kaskawulsh Glacier closest to the lake was separated from the rest of the glacier by large, arcuate fractures (Fig. 16). Kasper measured the vertical position of an array of targets on the ice-dam surface at three-dimensional intervals, and although the errors in those data are large, the pattern of vertical motion is strikingly similar to our findings at Kennicott Glacier. Two targets lakeward of the large arcuate fractures rose by an amount exceeding the increase of lake level (similar to our target LL1). The target closest to, but on the glacierward side of, the arcuate fractures rose by about 50% as much as lake level. Targets progressively farther from the lake showed progressively less uplift, falling off to practically zero over a few hundred meters. Moreover, the pattern of target downdrop during lake drainage mimicked the pattern of target uplift as the lake filled.

Origin of high-angle faults through the HCL ice dam

Aerial photographs of Kennicott Glacier show nearly the same pattern of fractures spanning the HCL ice dam from north to south from year to year. Bearing in mind that the front of the ice dam breaks up during lake drainage, there must be some mechanism that regenerates the fracture pattern. Our conception of this process is as follows. Fractures initially form in extension (as surface crevasses in the commonly understood sense) during lake drainage. In the 'far field' domain defined by R1, BL1 and MLN in 2000, say, there was extensional strain, $\dot{\varepsilon}$, at a rate of $\sim 0.1\,a^{-1}$ (Fig. 13), corresponding to a deviatoric stress $s = 2B\dot{\varepsilon}^{1/3}$ (e.g. Van der Veen, 1998b) of about 0.16 MPa, where we have taken $B = 5.3 \times 10^7$ Pa s$^{1/3}$ as the flow-law parameter for temperate ice (Paterson, 1994). The expected depth, d_c, of water-free crevasses is then 20–28 m, using $d_c = \tilde{k}(s/\rho_i g)$, where $g = 9.8\,m\,s^{-2}$ is acceleration due to gravity and $\tilde{k}$ ranges from 1 to $\pi/2$ depending upon crevasse spacing

(Weertman, 1973). These crevasses would be advected toward the lake basin and annually undergo a growth episode owing to two processes: impoundment of water within crevasses and enhanced extensional strain rate as the lake drains. Assuming that measured target speeds during the period of lake filling are characteristic for the entire year, which is probably an overestimate, it would take 4–6 years to advect a crevasse from an easting of 10000 (a bit east of R1) to an easting of 9800 (a bit east of M5). Furthermore, bottom crevasses are likely to grow wherever the subglacial water wedge lifts and bends the glacier by modest amounts during lake filling. Vertical-motion data (Fig. 11) indicate that the glacier became separated from the bed lakeward of about easting 9900. Confining stress on the basal ice in this part of the glacier would be near zero, and thus, as the ice was in extension, bottom crevasses could have readily formed, just as in a floating ice shelf (Van der Veen, 1998a). We suggest that these bottom crevasses link up with surface crevasses to form fractures penetrating through the entire glacier thickness. Such fractures are then advected toward the lake and act as high-angle faults during a subsequent cycle of lake filling and drainage. As noted above, the relative motion of targets lakeward of about easting 9700 appears to involve faulting. In this view, then, the ice dam within about 600 m of the lake behaves in important respects as a fractured brittle material rather than as a creeping plastic. We suggest that this part of the ice dam forms a compact mass as the lake fills because the valley walls buttress the fractured ice dam analogously to the way that constrictions in a river channel foster ice jams.

Significance of the time lag for downdrop

The time lag between lake drawdown and downdrop of the ice-dam surface (cf. Table 1) cannot be explained if we suppose that the ice dam is simply floating, in which case downdrop should track lake drawdown with no delay at all. An attempt at an explanation in terms of viscoelasticity is equally unsatisfactory. Simply put, a typical viscoelastic response time, τ_v, is of order η/Y, where η is an effective viscosity (Turcotte and Schubert, 1982). Treating the buoyant ice dam like a confined ice shelf, we may take $\eta \approx B^3/2s^2$, where s is the deviatoric stress associated with east–west extension of the ice dam (see, e.g., Van der Veen, 1999), and thus $\tau_v \approx B^3/2s^2 Y$. Taking the values for B, s and Y for intact ice given above, we find $\tau_v \approx 250$ s. To get τ_v close to the value of the time lag (typically 1–2 days, or roughly 10^5 s) would require reducing Y by a factor of 1000 compared to the value for intact glacier ice; however, this seems unlikely. This failure of a viscoelastic explanation is consistent with the failure of the flexural model.

The evidence for a pervasively faulted ice dam leads us to suggest that the time lag between the start of lake drawdown and the start of ice-surface drop may be the result of frictional resistance across faults and at the margins of the ice dam. As lake level begins to decrease, friction across a fault will keep a block that had been rising from immediately starting to drop. Downdrop of the block will not begin until the weight unsupported by buoyancy exceeds the frictional resistance across the fault. For simplicity, consider a section of the ice dam in the shape of a rectangular parallelepiped (box) with vertical extent H_i and dimensions L and W normal and parallel to the ice-dam face, respectively. If the average frictional stress across the vertical faces (both ice/ice and ice/rock) is τ_f, then downdrop should begin when

$$p_w(t)LW < \rho_i g H_i LW - 2\tau_f H_i(kW + L), \qquad (3)$$

where p_w is the average water pressure applied over the base of the ice block and $k = 1$ if the box is bounded by two faults, but $1/2$ if the box is bounded by a fault on one face and the lake on the opposite face. Recognizing that $\rho_i g H_i$ is the ice overburden pressure, $\rho_i g H_i - p_w(t)$ is then simply the weight per unit area unsupported by buoyancy as lake level drops. But $\rho_i g H_i - p_w(t) = \rho_w g \Delta h_w(t)$, where $\Delta h_w(t)$is the amount of drawdown. Thus ice-surface downdrop should not begin until $\Delta h_w > \Delta h_c$, where

$$\Delta h_c \approx \left(\frac{2\,\tau_f}{\rho_w g}\right) H_i \left(\frac{k}{L} + \frac{1}{W}\right). \qquad (4)$$

We make the usual assumption of Coulomb-frictional resistance on the vertical faces:

$$\tau_f \approx \mu \sigma_n, \qquad (5)$$

where the average frictional coefficient is μ and σ_n is the depth-averaged effective normal stress; thus

$$\Delta h_c \approx \left(\frac{2\,\sigma_n}{\rho_w g}\right) \mu H_i \left(\frac{k}{L} + \frac{1}{W}\right). \qquad (6)$$

As σ_n must be ≥ 0 (complete flotation) but $\leq \rho_i g H_i/2$ (no water pressure anywhere within the fault zone), the bounds on Δh_c are

$$0 \leq \Delta h_c \leq \mu \left(\frac{\rho_i}{\rho_w}\right) H_i^2 \left(\frac{k}{L} + \frac{1}{W}\right). \qquad (7)$$

As a specific example, consider the ice block lakeward of the fault that we believe separated targets F6, D1, F7, C2, F4, Rx, LL1 and M1 from targets C1 and M2 (in 2000), in which case $H_i \approx 250$ m, $W \approx 750$ m, $L \approx 600$ m and $k = 1/2$. We further choose $\mu \approx 1$ (reasonable for sea ice or pack ice on rivers; White, 1999) and $\rho_i/\rho_w = 0.9$ (probably a modest overestimate owing to the extent of crevassing). We then find $0 \leq \Delta h_c \leq 120$ m. Although we have no data bearing directly on the value of σ_n, the presence of water near the glacier surface in at least some crevasses supports the idea that σ_n must have been fairly small, and, indeed, the observed value $\Delta h_w \approx 2$ m at the start of ice-surface drop would indicate water pressure along faults of about 98% of the flotation value. Note also from Equation (7) that Δh_c is expected to increase with H_i, i.e. with distance from the lake, as is observed.

Significance of diurnal speed variations

An intriguing aspect of the motion data for both 1999 and 2000 is the diurnal variation in speed of targets on ice that is floating (or close to floating) and pervasively fractured, perhaps even faulted clear through from the surface to the bed in places. The floating part of the ice dam probably behaves roughly as a confined ice shelf, with the gravitational driving force balanced by drag on the sides and stress gradients within the ice (Van der Veen, 1999). As side drag is unlikely to vary diurnally, we suggest that diurnal variation in speed results from diurnal variation in stress gradients, with the ultimate source of such variations being the main body of the glacier. Changes in velocity boundary conditions are felt instantaneously through floating ice masses (Lange and MacAyeal, 1989). Thus, we might expect the timing of peaks in horizontal speed at a point on the main glacier to correlate with the timing of peaks in horizontal speed at

points on the ice dam. This conjecture is supported in a qualitative way by Figure 17. Speed variations of MLN, R1 and M4 are all clearly in phase. Rx, which lies lakeward of a major fault, was commonly but not always in phase with MLN. Even the near-lake target P2 showed a diurnal speed fluctuation, being consistently about 12 hours out of phase with MLN until sometime on day 192, when (as noted previously) the near-lake targets began to behave oddly. The irregular phasing of Rx, and the out-of-phase behavior of P2, must in some way reflect the mechanics of stress transmission across the faults and (possibly) between blocks of ice in the floating part of the ice dam nearest the lake.

Anomalous behavior of target LL1

As noted above, the movement of target LL1 was peculiar. LL1 rose at a rate substantially greater than the rate of lake-level change from day 190 until HCL drained (Fig. 12a). Moreover, LL1 initially diverged from Rx as the lake rose, then approached Rx as the lake drained (Fig. 14b), along a more-or-less reversible trajectory. Within the context of our faulted-ice-dam interpretation, we speculate that target LL1 was atop a local graben, a structure commonly associated with extensional tectonics and near-surface earth slumps (Varnes, 1978). Existence of a local graben could also explain why LL1 dropped so much more than other CC targets during lake drainage.

Possible role of ice-dam mechanics on jökulhlaup initiation and termination

To the extent that an ice dam behaves fundamentally as a fractured, rather than creeping, solid on the timescale relevant to lake filling and drainage, there may be significance for understanding aspects of lake drainage. Accepting the classic model of jökulhlaup initiation in the broadest sense, namely, that as lake level rises, the adjacent ice is lifted off its bed until a hydraulic seal is broken (Björnsson, 1974; Nye, 1976), then the integrity and mechanical behavior of the ice dam affects the critical lake level at which drainage begins. Nye (1976, p. 187) alluded to this idea and suggested that buoyancy forces would be transmitted laterally by flexure (thus his use of the phrase 'inverted cantilever', meaning, in his discussion, the floating ice shelf over the (mostly) subglacial lake Grímsvötn) and would reduce the lake level required to break the seal. If an ice dam is a fractured solid, however, the mechanics of stress transmission will be dominated by frictional effects. Just how this might affect the jökulhlaup-initiation condition is unclear, friction being a complicated phenomenon (Marone, 1998). A fractured ice dam could also affect jökulhlaup termination, perhaps most obviously if the drainage path becomes obstructed as fault-bounded ice blocks sag.

SUMMARY

We studied in detail the mechanical behavior of an 'ice dam', a small part of a glacier adjacent to an ice-marginal lake that fills and drains annually. Optical surveying revealed how the ice dam responded to varying lake level. Large vertical movements of the glacier surface are consistent with the idea that a wedge of water penetrates beneath the ice dam as the lake fills and that the ice dam is locally floating, or nearly so. The spatial pattern of vertical movement, however, cannot be explained by a flexural model of the sort used to account for tidally driven movement of floating glacier tongues and ice shelves. Observed deformation is instead best explained if the ice dam is locally faulted from the surface to the bed, through ~250–300 m of ice. The sense of slip on individual faults reverses direction as the lake drains. The faults, whose spatial pattern is practically the same from year to year, probably form by intersection of surface crevasses and basal crevasses. Diurnal fluctuations in the rate of ice-dam uplift cannot be explained if the only driving force for such motion is water pressure in the subglacial wedge. Even the highly fractured ice dam must also be responding to the gross dynamics of the main glacier.

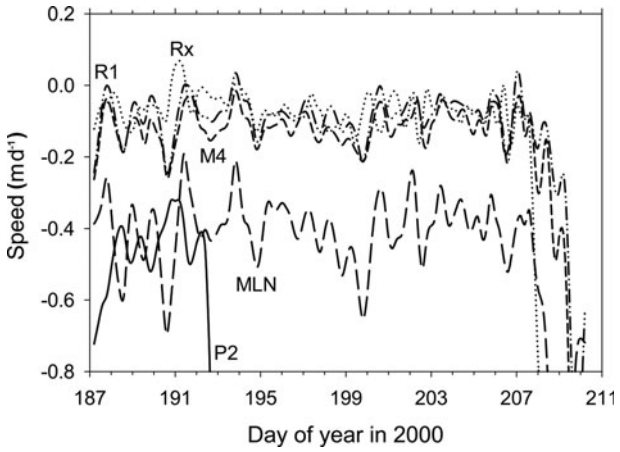

Fig. 17. Diurnal fluctuations in speed for several targets in 2000. Even targets on ice that was highly fractured displayed diurnal fluctuations.

ACKNOWLEDGEMENTS

D. Rosenkrans helped us obtain permission from Wrangell–St Elias National Park and Preserve to conduct this research. R. Jacobel provided radar equipment. J. Harper, D. Lindsay and R. Schlicting assisted in the field. F. Jones provided the photograph of Kaskawulsh Glacier. C.L. Hulbe, R.P. Denlinger, F.S. Tweed and an anonymous referee made valuable suggestions on the manuscript. Financial support was provided by the US National Science Foundation, Office of Polar Programs through grants 9812944, 9812945, 9812973, 9912129, 9912180 and 9912306.

REFERENCES

Anderson, R.S., J.S. Walder, S.P. Anderson, D.C. Trabant and A.G. Fountain. 2005. The dynamic response of Kennicott Glacier, Alaska, USA, to the Hidden Creek Lake outburst flood. *Ann. Glaciol.,* **40**, 237–242.

Anderson, S.P. *and 6 others*. 2003a. Integrated hydrologic and hydrochemical observations of Hidden Creek Lake jökulhlaups, Kennicott Glacier, Alaska. *J. Geophys. Res.,* **108**(F1), 6003. (10.1029/2002JF000004.)

Anderson, S.P., S.A. Longacre and E.R. Kraal. 2003b. Patterns of water chemistry and discharge in the glacier-fed Kennicott River, Alaska: evidence for subglacial water storage cycles. *Chem. Geol.,* **202**(3–4), 297–312.

Björnsson, H. 1974. Explanation of jökulhlaups from Grímsvötn, Vatnajökull, Iceland. *Jökull,* **24**, 1–26.

Björnsson, H. 1992. Jökulhlaups in Iceland: prediction, characteristics and simulation. *Ann. Glaciol.,* **16**, 95–106.

Björnsson, H. 2002. Subglacial lakes and jökulhlaups in Iceland. *Global Planet. Change,* **35**(3–4), 255–271.

Clague, J.J. and W.H. Mathews. 1973. The magnitude of jökulhlaups. *J. Glaciol.,* **12**(66), 501–504.

Cunico, M.L. 2003. Ice deformation associated with a glacier-dammed lake in Alaska and the implications for outburst flood hydraulics. (MS thesis, Portland State University.)

Fowler, A.C. 1999. Breaking the seal at Grímsvötn, Iceland. *J. Glaciol.,* **45**(151), 506–516.

Friend, D.A. 1988. Glacial outburst floods of the Kennicott Glacier, Alaska – an empirical test. (MA thesis, University of Colorado, Boulder.)

Guðmundsson, M.T., F. Sigmundsson, H. Björnsson and þ. Högnadóttir. 2004. The 1996 eruption at Gjálp, Vatnajökull ice cap, Iceland: efficiency of heat transfer, ice deformation and subglacial water pressure. *Bull. Volcanol.,* **66**(1), 46–65.

Huss, M., A. Bauder, S. Sugiyama, M. Werder and M. Funk. 2006. Glacier dammed lake outburst events of Gornersee, Switzerland. *Geophys. Res. Abstr.* 8, 00533. (1607-7962/gra/EGU06-A-00533.)

Kasper, J.N. 1989. An ice-dammed lake in the St. Elias Range, southwestern Yukon Territory: water balance, physical limnology, ice dynamics and sedimentary processes. (MA thesis, Ottawa University.)

Lange, M.A. and D.R. MacAyeal. 1989. Numerical models of ice-shelf flow: ideal/real. *Ann. Glaciol.,* **12**, 97–103.

Lingle, C.S., T.J. Hughes and R.C. Kollmeyer. 1981. Tidal flexure of Jakobshavns glacier, West Greenland. *J. Geophys. Res.,* **86**(B5), 3960–3968.

Marone, C. 1998. Laboratory-derived friction laws and their application to seismic faulting. *Annu. Rev. Earth Planet. Sci.,* **26**, 643–696.

Ng, F. and H. Björnsson. 2003. On the Clague–Mathews relation for jökulhlaups. *J. Glaciol.,* **49**(165), 161–172.

Nye, J.F. 1976. Water flow in glaciers: jökulhlaups, tunnels and veins. *J. Glaciol.,* **17**(76), 181–207.

Old, G.H., D.M. Lawler and Á. Snorrason. 2005. Discharge and suspended sediment dynamics during two jökulhaups in the Skaftá river, Iceland. *Earth Surf. Process. Landf.,* **30**(11), 1441–1460.

Paterson, W.S.B. 1994. *The physics of glaciers. Third edition.* Oxford, etc., Elsevier.

Post, A. and L.R. Mayo. 1971. Glacier dammed lakes and outburst floods in Alaska. *USGS Hydrol. Invest. Atlas* HA-455.

Rickman, R.L. and D.S. Rosenkrans. 1997. Hydrologic conditions and hazards in the Kennicott River Basin, Wrangell–St. Elias National Park and Preserve, Alaska. *USGS Water Resour. Invest. Rep.* 96–4296.

Roberts, M.J. 2005. Jökulhlaups: a reassessment of floodwater flow through glaciers. *Rev. Geophys.,* **43**, RG1002. (10.1029/2003RG000147.)

Russell, A.J., F.S. Tweed, O. Knudsen, M.J. Roberts, T.D. Harris and P.M. Marren. 2002. Impact of the July 1999 jökulhlaup on the proximal river Jökulsá á Sölheimasandi, Mýrdalsjökull glacier, southern Iceland. *IAHS Publ.* 271 (Symposium at Reykjavík 2000 – *Extremes of the Extremes*), 249–254.

Sugiyama, S. *and 8 others.* 2005. Glacier dynamics during the outburst flood of a glacier dammed lake on Gornergletscher, Switzerland. *Geophys. Res. Abstr.* 7, 07473. (1607-7962/gra/EGU05-A-07473.)

Turcotte, D.L. and G. Schubert. 1982. *Geodynamics: applications of continuum physics to geological problems.* New York, etc., John Wiley and Sons.

Van der Veen, C.J. 1998a. Fracture mechanics approach to penetration of bottom crevasses on glaciers. *Cold Reg. Sci. Technol.,* **27**(3), 213–223.

Van der Veen, C.J. 1998b. Fracture mechanics approach to penetration of surface crevasses on glaciers. *Cold Reg. Sci. Technol.,* **27**(1), 31–47.

Van der Veen, C.J. 1999. *Fundamentals of glacier dynamics.* Rotterdam, etc., A.A. Balkema Publishers.

Varnes, D.L. 1978. Slope movement and types and processes. *In* Schuster, R.L. and R.J. Krizek, *eds. Landslides – analysis and control.* Washington, DC, National Academy of Sciences. National Research Council, Transportation Research Board, 12–33. (Special report 176.)

Walder, J.S. and J.E. Costa. 1996. Outburst floods from glacier-dammed lakes: the effect of mode of lake drainage on flood magnitude. *Earth Surf. Process. Landf.,* **21**(8), 701–723.

Walder, J.S., D.C. Trabant, M. Cunico, S.P. Anderson, R.S. Anderson and A.G. Fountain. 2005. Fault-dominated deformation in an ice dam during annual filling and drainage of a marginal lake. *Ann. Glaciol.,* **40**, 174–178.

Weertman, J. 1973. Can a water-filled crevasse reach the bottom surface of a glacier? *IASH Publ.* 95 (Symposium at Cambridge 1969 – *Hydrology of Glaciers*), 139–145.

Werder, M.A. *and 6 others.* 2006. Glacier dammed lake outburst events of Gornersee, Switzerland Part II. *Geophys. Res. Abstr.,* 8, 06645. (1607-7962/gra/EGU06-A-06645

White, K.D. 1999. Hydraulic and physical properties affecting ice jams. *CRREL Rep.*

MS received 14 December 2005 and accepted in revised form 24 June 2006